Journal of Applied Physics

RESEARCH ARTICLE | NOVEMBER 08 2019

Tunable magnetic domain walls for therapeutic neuromodulation at cellular level: Stimulating neurons through magnetic domain walls

Diqing Su ; Kai Wu ; Renata Saha ; Jian-Ping Wang

J. Appl. Phys. 126, 183902 (2019)
https://doi.org/10.1063/1.5122753
CHORUS

Journal of Applied Physics ARTICLE scitation.org/journal/jap

Tunable magnetic domain walls for therapeutic neuromodulation at cellular level: Stimulating neurons through magnetic domain walls

Cite as: J. Appl. Phys. **126**, 183902 (2019); doi: 10.1063/1.5122753
Submitted: 2 August 2019 · Accepted: 17 October 2019 ·
Published Online: 8 November 2019

Diqing Su,[1,a] Kai Wu,[2,a] Renata Saha,[2] and Jian-Ping Wang[2,b]

AFFILIATIONS

[1]Department of Chemical Engineering and Material Science, University of Minnesota, Minneapolis, Minnesota 55455, USA
[2]Department of Electrical and Computer Engineering, University of Minnesota, Minneapolis, Minnesota 55455, USA

[a]**Contributions:** D. Su and K. Wu contributed equally to this work.
[b]**Author to whom correspondence should be addressed:** jpwang@umn.edu

ABSTRACT

Cellular-level neuron stimulation has attracted much attention in the areas of prevention, diagnosis, and treatment of neurological disorders. Herein, we propose a spintronic neurostimulator based on the domain wall movement inside stationary magnetic nanostructures driven by the spin transfer torques. The electromotive forces generated by the domain wall motion can serve as highly localized stimulation signals for neuron cells. Our simulation results show that the induced electric field from the domain wall motion in permalloy nanostructures can reach up to 14 V/m, which is well above the reported threshold stimulation signal for clinical applications. The proposed device operates on a current range of several microamperes that is 10^3 times lower than the current needed for the magnetic stimulation by microcoils. The duration and amplitude of the stimulating signal can be controlled by adjusting the applied current density, the geometry of the nanostructure, and the magnetic properties of the material.

I. INTRODUCTION

In 2013, the National Institutes of Health (NIH), the Defense Advanced Research Projects Agency (DARPA), and the National Science Foundation (NSF) launched a project named the BRAIN Initiative[1,2] to accomplish the prevention, diagnosis, and treatment of brain disorders such as Alzheimer's disease, attention deficit hyperactivity disorder (ADHD), Parkinson's disease, migraines, and traumatic brain injury (TBI). The primary challenge in this process is the lack of understanding of the pathogenesis, which makes it necessary to investigate the interactions within the brain from the cellular level to the complex neural circuits through brain stimulation. Since the early work of Wise *et al.*,[3] research studies in neuroscience and neural engineering have experienced rapid growth, especially in exploring new probe materials and new fabrication technologies to produce miniaturized, customized, and high-density electrode arrays for the stimulation of neurons. Despite their great potential, the electrode arrays employed in most of the current brain stimulation technologies are constantly affected by the migration of cells (such as astrocytes) around the devices, which leads to increased impedance and alterations of the electric field in the stimulation processes. One way to avoid the influence of surrounding neuron cells on the stimulation signal is magnetic stimulation, where a magnetic field is generated and is not affected by the encapsulation of astrocytes or any other cells. Transcranial magnetic stimulation (TMS) is a commonly used noninvasive brain stimulation technique that utilizes a strong alternating magnetic field (1.5 T to 3 T) to modulate the neuron activities.[4–6] However, due to the bulky and noninvasive nature of this setup, it is impossible to generate a highly focused magnetic field. Moreover, as the magnetic field decays exponentially over distance, this technique cannot stimulate neurons located deep inside the brain. As a complementation of TMS, deep brain stimulation (DBS) implants electrodes in certain regions of the brain permanently to activate deeply located neurons.[7–9] Nevertheless, heating effects and large power consumption due to the constant application of relatively large-amplitude current are major drawbacks of DBS. Consequently, the development of an

implantable magnetic neurostimulator with the ability of generating a highly localized magnetic field through a low power input is essential for both the study of neuron activities and the treatment of neuron disorders.

The domain walls (DWs) from magnetic nanostructures are promising candidates for the magnetic stimulation of neuron cells.[10] The displacement of magnetic domain walls through the current has been widely studied to switch local magnetization in high-density magnetic recording applications.[11–13] The velocity of the domain walls can be controlled by the applied current density. Pulses of highly spin polarized current can move the entire pattern of DWs coherently along the nanostructure. A neuron cell placed at a certain location on top of the nanostructure will be stimulated with an electromotive force (EMF) that is induced by the change of the magnetic stray field generated by the domain wall movement within the nanostructure. Since the width of the domain wall ranges from the nanometer scale to the submicrometer scale, the stimulation is highly localized and is free from the influence of the surrounding environment, which facilitates neuron stimulation at the cellular level. Like the electrical stimulators, special attention needs to be paid to the biotoxicity of the magnetic stimulators since most of the magnetic materials are also highly toxic. As a result, passivation techniques are required to isolate the magnetic materials from the neuron cells. It has been shown that neuron cells can be successfully grown on the surface of the magnetic tunnel junctions passivated with $SiO_2/Si_3N_4/SiO_2$.[14] In addition, since the magnetic stimulator arrays are fully compatible with most of the fabrication processes for electrical stimulators, various passivation materials employed in the electrical stimulators such as polydimethylsiloxane (PDMS),[15] poly(3,4-ethylenedioxythiophene) (PEDOT),[16] and SiC[17] can also be applied to the magnetic stimulators. In this paper, we have theoretically demonstrated the feasibility of stimulating an individual neuron under adjustable magnetic field strength and frequency with nanofabricated magnetic nanostructure arrays (Fig. 1).

II. METHODS

The magnetic dynamics including spin transfer torque (STT) terms with an extended Landau-Lifshitz-Gilbert (LLG) equation is used in the simulation, which can be expressed as

$$\frac{d\boldsymbol{m}}{dt} = \gamma_0 \boldsymbol{H}_{eff} \times \boldsymbol{m} + \alpha \boldsymbol{m} \times \frac{d\boldsymbol{m}}{dt} - (\boldsymbol{u}\cdot\nabla)\boldsymbol{m} + \beta \boldsymbol{m} \times (\boldsymbol{u}\cdot\nabla)\boldsymbol{m}, \quad (1)$$

$$\boldsymbol{u} = \frac{\boldsymbol{J}_c P g \mu_B}{2eM_s}, \quad (2)$$

where $\boldsymbol{m} = \frac{\boldsymbol{M}}{M_s}$ is the unit magnetization vector, M_s is the saturation magnetization, $\boldsymbol{H}_{eff}$ is the effective magnetic field, γ_0 is the absolute value of the gyromagnetic ratio, and α is the Gilbert damping parameter. The last two terms on the right side of Eq. (1) are adiabatic and nonadiabatic torque terms. The dimensionless quantity β represents the degree of nonadiabaticity, $\boldsymbol{u}$ (in m/s) is the effective drift velocity of the conduction electron spins, $\boldsymbol{J}_C$ is the charge current density, P is the spin polarization of the current, g is the Landé factor, μ_B is Bohr magneton, and e is the electron charge. Here, we consider the permalloy ($Ni_{80}Fe_{20}$) nanostructure with the current applied along the wire axis, and the material parameters are assumed as follows: $\alpha = 0.02$, $\beta = 0.04$, $M_s = 8 \times 10^5$ A/m, $P = 0.6$, and exchange constant $A = 20$ pJ/m that gives an exchange length of 5 nm. The permalloy nanostructure has dimensions of $10\,\mu\text{m} \times 8\,\text{nm} \times 8\,\text{nm}$, and the simulation cell size is set to be $2 \times 2 \times 2\,\text{nm}^3$ (Table I). We used the object oriented micromagnetic framework (OOMMF)[18] code for simulations that solve the LLG equation incorporating the STT terms.

Based on the Maxwell-Faraday law, alternating magnetic flux density can induce an electromotive force (EMF),

$$\oint \boldsymbol{E}\cdot d\boldsymbol{l} = -\iint \frac{\partial \boldsymbol{B}}{\partial t}\cdot d\boldsymbol{S}, \quad (3)$$

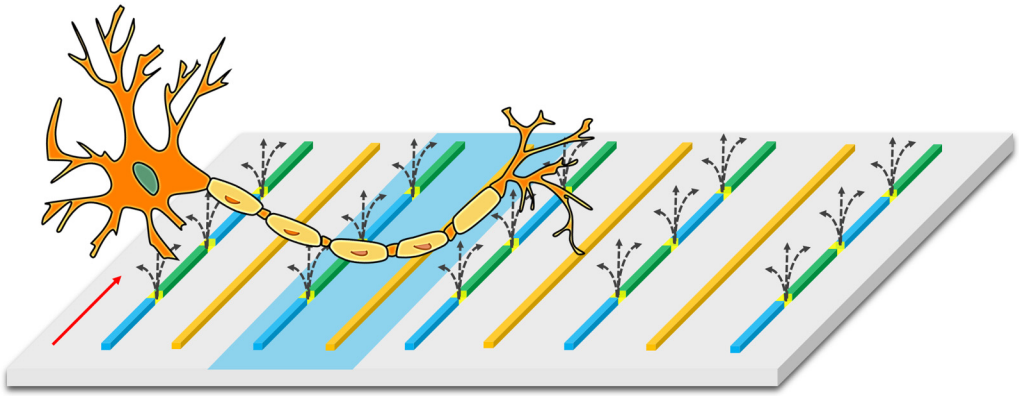

FIG. 1. Schematic illustration of the on-chip magnetic stimulation and sensing of a neuron cell. The device is designed to be implanted *in vivo* with passivation materials coated on the surface. The region highlighted in blue consists of a magnetic stimulator (left) and a magnetic nanosensor (right). There are multiple domain walls in the stimulation device, which can generate the electromotive forces. Different parts of the neuron cell can be stimulated by multiple magnetic stimulators, and the resulting magnetic field generated within the neuron after the stimulation will be sensed by the magnetic nanosensor adjacent to the magnetic stimulator. The red arrow indicates the direction of the applied current.

TABLE I. Simulation parameters of the magnetic domain wall movement in permalloy nanostructures.

Parameter	Description	Value
Dimensions	Length × Width × Thickness	$10\,\mu m \times 8\,nm \times 8\,nm$
Cell size	Length × Width × Thickness	$2 \times 2 \times 2\,nm^3$
α	Gilbert damping factor	0.02
β	Nonadiabatic spin transfer torque factor	0.04
A	Exchange constant	20×10^{-12} J/m
P	Polarization factor	0.6
M_s	Saturation magnetization	0.8×10^6 A/m
J_C	Charge current density	$10^{11} - 2.4 \times 10^{13}$ A/m^2
I	Charge current	$6.4\,\mu A$–1.5 mA

where B is the magnetic flux density, E is the electric field, l is the contour, and S is the surface area. It is reported that the neuron cells can be stimulated by an electric field higher than 10 V/m with duration longer than $50\,\mu s$[19–22] This can be determined by the domain wall velocity and can, thus, be controlled by the applied current density.

III. RESULTS AND DISCUSSION

A. Generation of highly localized magnetic field

As shown in Fig. 2(a), due to large shape anisotropy, the magnetizations in the domains of a magnetic nanostructure with very high aspect ratio ($10\,\mu m$:8 nm) tend to lie along the long axis (x axis), resulting in negligible short axis (y or z axis) components of the stray field. To minimize the total energy, there are usually multiple domains in the nanostructure, which are separated by the domain walls. As the magnetizations rotate either toward y or z direction within the domain wall, the y or z components of the stray field become nonzero. During the current-driven domain wall motion, the stray field experienced by a neuron cell located at a fixed location in proximity to the nanostructure surface will either increase or decrease, generating an electromotive force, i.e., a stimulation signal. Without further notation, the stray field in the following content refers to the stray field perpendicular to the nanostructure surface (H_z) that is used to generate the stimulation signal. Since the structure of the nanomaterial is symmetrical in the y and z direction, the analysis of the stray field in the y direction should be similar to that in the z direction and, thus, will not be discussed again in this paper.

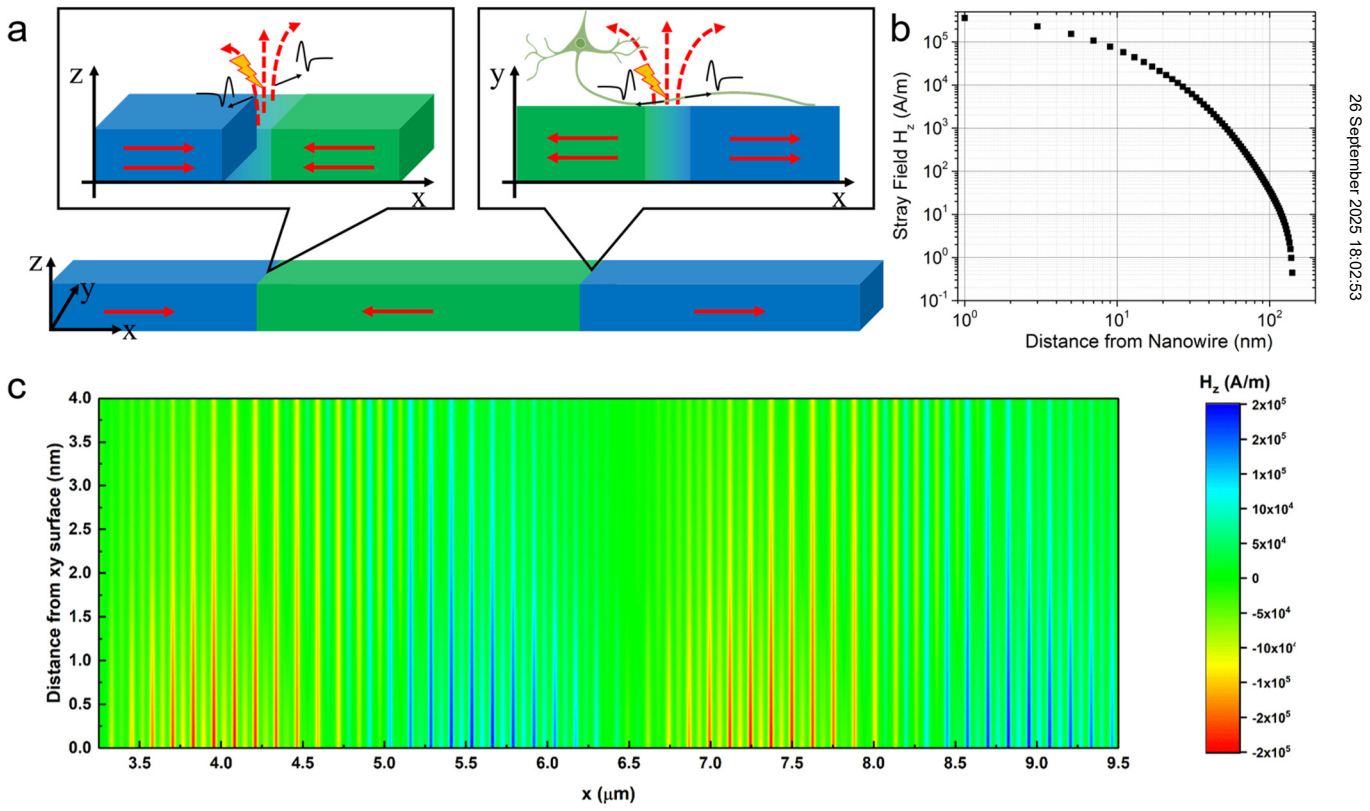

FIG. 2. (a) Schematic view of different magnetic domain walls in a magnetic nanostructure: (i) perpendicular transverse wall and (ii) transverse wall. Red arrow represents the magnetization in that domain. (b) Out-of-plane magnetic stray field component H_z attenuates from 320 kA/m at the surface of the nanostructure to below 1 A/m at 150 nm from the surface. (c) The z component of the stray field H_z across the nanostructure as a function of the distance from the xy surface.

To realize cellular-level neuron stimulation, the out-of-plane stray field should be highly localized around the domain wall, which is determined by the fast decay of the stray field and the width of the domain wall. The amplitude of the stray field along the z direction (H_z) is plotted against the distance from the nanostructure surface in Fig. 2(b). The maximum stray field at the surface of the nanostructure is 3.2×10^5 A/m, which is in the same order of the saturation magnetization (8×10^5 A/m) and decays to less than 1 A/m at a distance of 150 nm. Since the size of the neuron cells is in the micrometer range, while the thickness of the cell membranes is in the order of several nanometers, the distribution of the domain wall stray field can penetrate the membrane of the cell on top of its surface without further influence on other surrounding cells, which makes it possible to realize single-cell stimulation. Based on this argument, the calculation of the electrical stimulation signal in the subsequent section will be focused only in the region within the width of the domain wall. Furthermore, magnetic nanostructures in the array can be controlled by separate electrodes with only one nanostructure activated each time so that other neurons located in proximity to other nanostructures will not be stimulated. The distribution of the stray field in the transverse direction is determined by the domain wall width. The width of the domain wall is around 40 nm for a permalloy nanostructure with a thickness of 8 nm as observed in our simulation, which is consistent with the previously reported value and can be adjusted by simply altering the geometry of the nanostructure.[23] This facilitates the highly localized stimulation at a specific spot of the neuron cells. As shown in Fig. 2(c), H_z is nonzero within each domain wall in the nanostructure and decays to zero at the edges of the domain wall. The amplitude of H_z is different at each domain wall due to the difference in the magnetization orientation within the wall, which will be discussed in Sec. III B. Due to the nanoscale domain structure of the permalloy nanostructure and the fast decay of the magnetic field in nonmagnetic space, a highly localized stimulation signal can be generated, whose viable stimulation region can be modified by multiple parameters, including the exchange constant and the anisotropy constant of the nanostructure material as well as the geometry of the nanostructures.

B. Current-driven domain wall motion

To induce a change in the stray field, a spin polarized current is applied to the nanostructure. Driven by the spin transfer torque, the magnetic domain wall moves along the +x direction, which can be characterized by the change in the distribution of the demagnetization field profile along the nanostructure at different timepoints. The system is stabilized for 25 ns after the application of the current (see Fig. S1 in the supplementary material). As shown in Fig. 3(a), the demagnetization field distributions are plotted at different locations along the long axis of the nanostructure every 0.15 ns. The applied current J is 1.2×10^{13} A/m^2, which corresponds to an effective drift velocity u of 600 m/s. Each peak in the

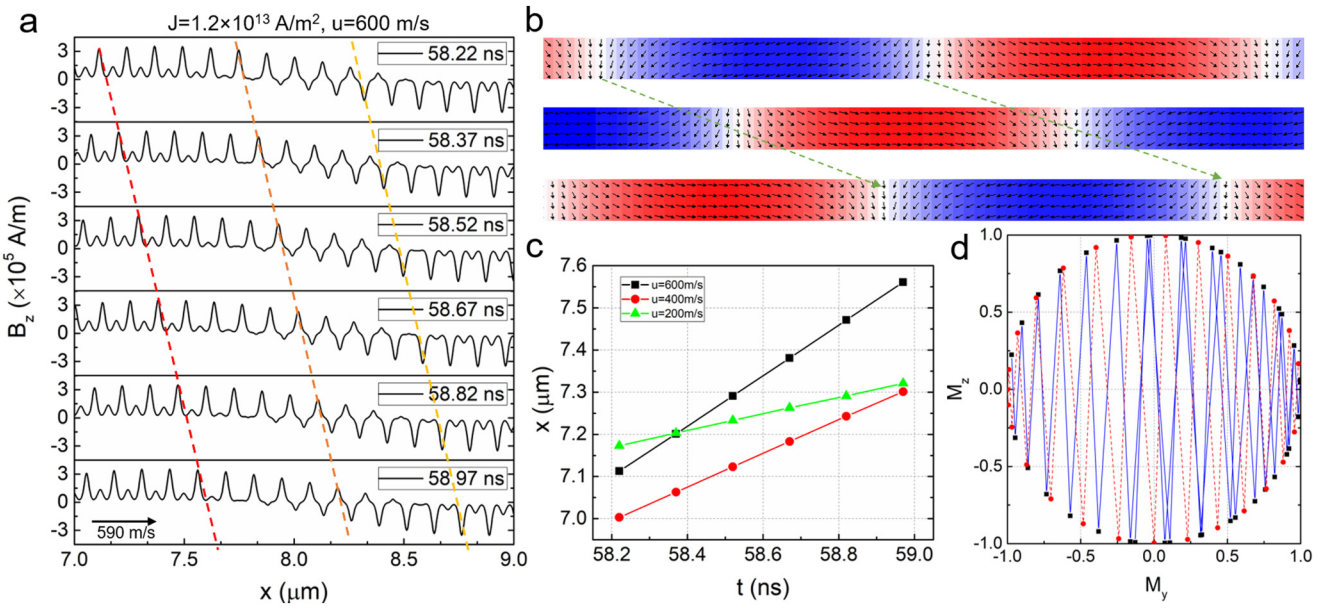

FIG. 3. (a) Distribution of the demagnetization field along the center line of the nanostructure ($y = 4$ nm, $z = 4$ nm) at $t = 58.22$ ns, 58.37 ns, 58.52 ns, 58.67 ns, 58.82 ns, and 58.97 ns under an applied current of 1.2×10^{13} A/m^2. The red, orange, and yellow lines connect the locations of one domain wall at different timepoints, indicating linear displacements of the domain wall. The domain wall velocity is calculated to be 590 m/s. (b) Magnetization distribution in the nanostructure at $t = 58.22$ ns, 58.37 ns, and 58.52 ns under an applied current of 1.2×10^{13} A/m^2. The green arrow indicates the movement of the domain walls. (c) Domain wall position at different timepoints for $u = 200$ m/s, 400 m/s, and 600 m/s. (d) Magnetization in the y and z direction at the cross section of each domain wall along the x axis under an applied current density of 1.2×10^{13} A/m^2. The blue line indicates the oscillation of the domain wall magnetization for domain walls located at $x = 4.019\,\mu$m – $4.845\,\mu$m. The red line indicates the oscillation of the domain wall magnetization for domain walls located at $x = 2.565\,\mu$m –$3.201\,\mu$m.

profile represents one domain wall, and all the domain walls move toward +x direction consistently after the application of the spin polarized current, which can also be confirmed by the magnetization distribution presented in Fig. 3(b). The domain wall profiles for $u = 400\,\mathrm{m/s}$ and $u = 200\,\mathrm{m/s}$, which correspond to current densities of $8 \times 10^{12}\,\mathrm{A/m^2}$ and $4 \times 10^{12}\,\mathrm{A/m^2}$, also exhibit a similar trend as shown in Fig. S2 in the supplementary material. By plotting the locations of one domain wall in the nanostructure at different timepoints, the domain wall velocities v under different applied currents can be calculated, which turn out to be 200 m/s, 400 m/s, and 590 m/s under current densities of $4 \times 10^{12}\,\mathrm{A/m^2}$, $8 \times 10^{12}\,\mathrm{A/m^2}$, and $1.2 \times 10^{13}\,\mathrm{A/m^2}$, respectively [Fig. 3(c)]. It is observed that $v \approx u$ for the utilized current densities, which is in accordance with the results from other literatures when the current is above the threshold current, also known as Walker limit.[24–26] In this case, the Walker limit is estimated to be $2 \times 10^{10}\,\mathrm{A/m^2}$.[24]

For transverse domain walls, when the applied current is below the Walker limit, the spin transfer torque is counteracted by damping, which cants the spin out of the plane.[27] Once the current is above the Walker limit, the spin transfer torque will be much larger than the torque due to damping, driving the domain walls to move continuously while precessing around the x axis. The rotation of domain wall planes can be confirmed by the inconsistent peak values of B_z in Fig. 3(a). As shown in Fig. 3(d), the magnetizations at the center of the domain wall oscillate around the z axis. Since the domain walls move at a constant velocity, this effect can also be viewed as the oscillation of the domain wall planes for a given location along the nanostructure at different timepoints, which is confirmed by the projection of magnetizations in the $M_y - M_z$ plane in Fig. 4(a). The reason behind this oscillation pattern can be explained qualitatively as follows. Due to dipolar interaction, the magnetizations at the end of the nanostructure tend to tilt away from the x axis. According to the first term of the LLG equation, $\gamma_0 \boldsymbol{H}_{eff} \times \boldsymbol{m}$, where $\boldsymbol{H}_{eff}$ mainly consists of the demagnetization field, the magnetizations at the end of the nanostructure precess around the x axis. When the damping term is taken into consideration, the magnetizations will be pushed toward the x axis with a decreasing precession angle. The spin transfer torque is either in the same or in the opposite direction of the damping term depending on the direction of the applied current, which will either move the magnetizations toward or against the x axis.[28] Upon the application of the spin polarized current, the nonzero y and z components of the magnetizations can be transferred into the nanostructure. Consequently, the end of the nanostructure can be viewed as a domain wall generator. Since the domain walls are constantly injected into the nanostructure by the current, the equilibrium domain wall structure will depend on the possible configurations of adjacent domain walls upon collisions. According to Kunz,[29] two domain walls can either annihilate with each other or form a stabilized structure depending on the types of topological defects. It was shown that only domain walls with the same topological charges can be preserved during the collision, resulting in a 360° domain wall, while the domain walls with opposite topological charges will annihilate, forming a single domain. In our cases, only adjacent domain walls with opposite signs of m_z can survive, which explains the oscillation of domain wall planes around the z axis. As a result of the domain wall rotation, the demagnetization field generated by the domain wall along the y and z direction exhibits a

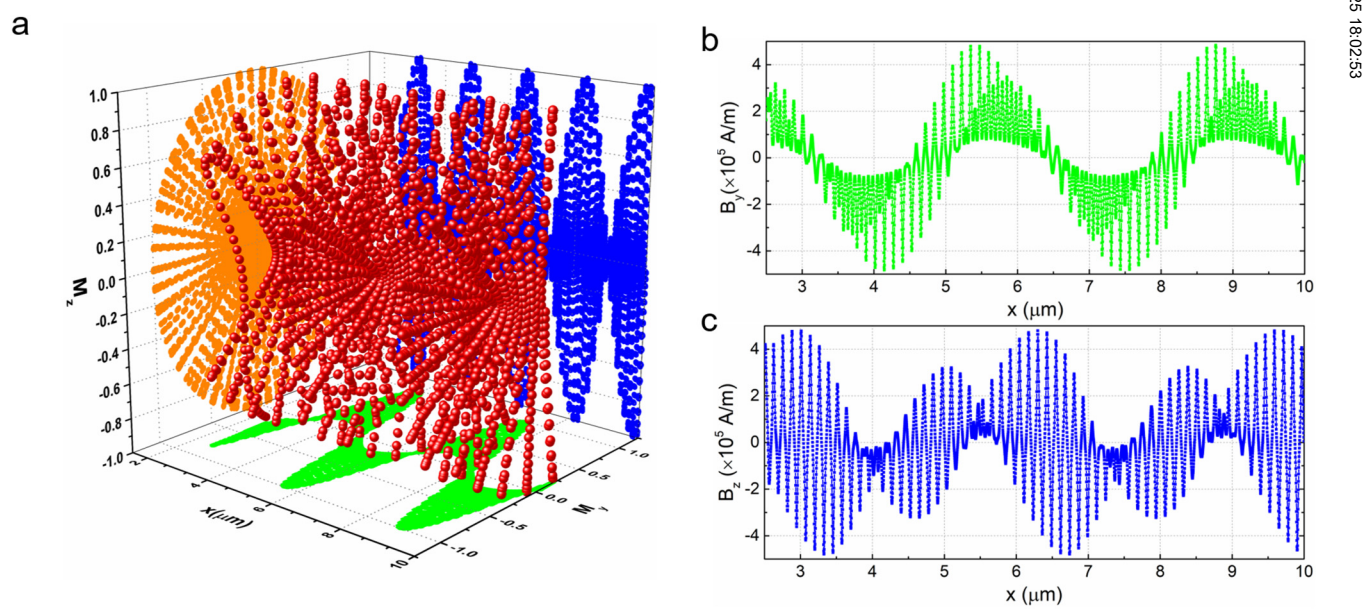

FIG. 4. (a) Three-dimensional plot of the magnetizations at the center of the nanostructure under an applied current of $1.2 \times 10^{13}\,\mathrm{A/m^2}$. The projection in the $x - M_y$, $x - M_z$, and $M_y - M_z$ planes are also shown. The distributions of the demagnetization field B_y (b) and B_z (c) along the x axis are calculated from (a).

wavelike form, as shown in Figs. 4(b) and 4(c), where the frequency of the oscillation is determined by the distance between adjacent domain walls and the velocity of the domain walls.

C. Electromotive force for neuron stimulation

According to Faraday's law, the alternating stray fields from the nanostructure can generate electromotive forces. Assuming that the contour of E field is a circle with a diameter comparable to the width of the domain wall, the Faraday's law can be rewritten as

$$2\pi rE = -\frac{\Delta B}{\Delta t}\pi r^2, \tag{4}$$

which gives

$$E = -\frac{r}{2}\frac{\Delta B}{\Delta t}, \tag{5}$$

with $v = \frac{r}{\Delta t}$,

$$E = -\frac{v}{2}\Delta B, \tag{6}$$

where E is the electrical field, B is the stray field from the domain wall, r is half of the width of the domain wall, Δt is the time difference between two adjacent data points, and v is the velocity of the domain wall motion. The instantaneous electrical field is proportional to the change of the stray field and the domain wall velocity and, thus, can be adjusted by tuning the magnetic properties of the nanostructure material or, more conveniently, the applied current density. The calculated electromotive force at the surface of a permalloy nanostructure under an applied current of 1.2×10^{13} A/m^2 is shown in Fig. 5. Since the domain walls are moving at a constant velocity, the spatial distribution of the electrical field can be converted to the time domain. Like the patterns of the stray field, both electromotive forces along the y and z axis exhibit wavelike behaviors with a maximum electrical field of 14 V/m, which is larger than the minimum requirement for neuron modulation (5 V/m).[20] It is worth noting that the threshold electrical field may vary with the pulse width of the stimulation signal.[30] Here, the frequency of the stimulation signal is 4.76 GHz. When the applied current densities are decreased to 8×10^{12} A/m^2 and 4×10^{12} A/m^2, the amplitudes of the stimulation signal are decreased to 7.8 V/m and 3.8 V/m, respectively, and the frequencies are decreased to 2.86 GHz and 2.78 GHz, respectively. The magnitude of the stimulation signal needs to be adjusted according to different clinical applications by changing the applied current density, the geometry of the nanostructure, and/or the magnetic properties of the material. Since the domain wall motion can be continuously driven by the spin polarized current, the duration of the signal can be easily controlled by turning the current on and off. Based on the application, an alternating current with high frequency can also be employed to obtain the required pattern of the stimulation signal. The commonly used neuron stimulation technologies such as electrical current-based DBS and microcoil require electrical currents in the milliampere range,[31,32] which is not only power consuming but can also lead to heating effects. Domain wall-based spintronic neuron stimulation, however, only requires current densities of

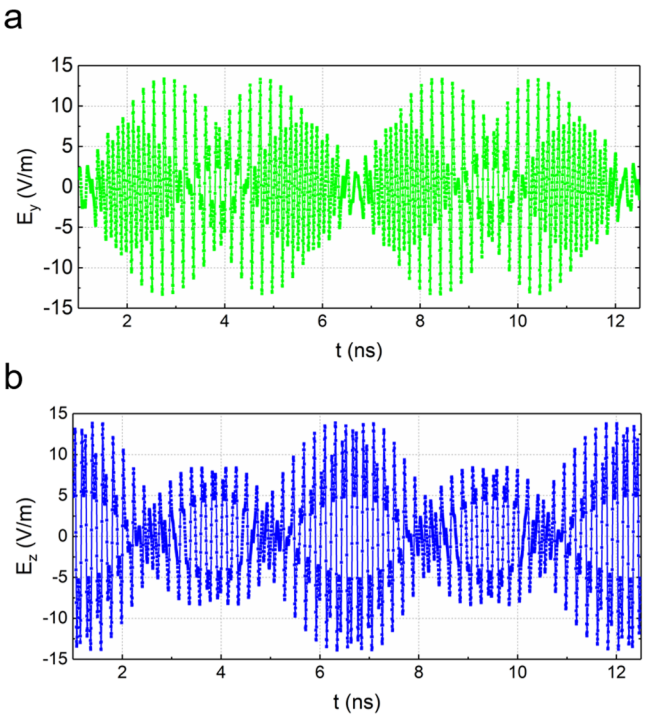

FIG. 5. The electrical field generated by the alternating stray field during the domain wall motion along the (a) y axis and (b) z axis under an applied current density of 1.2×10^{13} A/m^2.

10^{12}-10^{13} A/m^2, which corresponds to currents in the microampere range. The corresponding power consumptions within the nanostructure are calculated to be 27.7 mW, 12.3 mW, and 3.08 mW under the applied currents of 1.2×10^{13} A/m^2, 8×10^{12} A/m^2, and 4×10^{12} A/m^2, respectively.

IV. CONCLUSIONS

Current neuron modulation technologies suffer from multiple problems such as encapsulation of cells around the devices, bulky equipment, large power consumption, and heating effects. Magnetic domain wall-based stimulation was studied in this letter as a potential candidate with the capability of overcoming these difficulties. When the applied electrical current is above the Walker limit, the magnetic domain walls within the nanostructure can move at a constant velocity comparable to the drift velocity of the conduction electron spins. Due to domain wall rotation, the stray fields generated by the domain walls exhibit wavelike patterns along the nanostructure. The resulting electromotive force from the domain wall motion has a maximum amplitude of 14 V/m with a frequency of 4.76 GHz. With the application of domain wall-based spintronic nanodevices, the required electrical current can be reduced from tens of milliamperes to several microamperes, which significantly reduces the power consumption and the heating effects. Based on the specific requirements of clinical applications,

the frequency and amplitude of the stimulation signal can be adjusted by altering the frequency and amplitude of the applied current, the geometry of the nanostructure, and the magnetic properties of the nanostructure material. Since these neuron stimulators can be fabricated with microfabrication techniques, they can be easily integrated with other functional devices such as magnetic nanosensors on flexible substrates to realize stimulation and detection on a single chip.

SUPPLEMENTARY MATERIAL

See the supplementary material for the simulation results under other electrical current densities.

ACKNOWLEDGMENTS

This study was financially supported by the Institute of Engineering in Medicine of the University of Minnesota through FY18 IEM Seed Grant Funding Program, the National Science Foundation MRSEC Facility Program, the Centennial Chair Professorship, and Robert F. Hartmann Endowed Chair from the University of Minnesota. The authors declare no conflict of interest.

REFERENCES

[1]T. R. Insel, S. C. Landis, and F. S. Collins, Science **340**, 687 (2013).
[2]C. Bargmann *et al.*, Brain Research Through Advancing Innovative Neurotechnologies (BRAIN) Working Group Report to the Advisory Committee to the Director, NIH, US National Institutes of Health, 2014, see http://www.nih.gov/science/brain/2025/.
[3]K. D. Wise, J. B. Angell, and A. Starr, IEEE Trans. Biomed. Eng. BME-17, 238 (1970).
[4]R. Chen, J. Classen, C. Gerloff, P. Celnik, E. M. Wassermann, M. Hallett, and L. G. Cohen, Neurology **48**, 1398 (1997).
[5]M. Hallett, Nature **406**, 147 (2000).
[6]S. Tremblay *et al.*, Clin. Neurophysiol. **130**, 802 (2019).
[7]G. Deuschl *et al.*, N. Engl. J. Med. **355**, 896 (2006).
[8]A. L. Benabid, P. Pollak, D. M. Gao, D. Hoffmann, P. Limousin, E. Gay, I. Payen, and A. Benazzouz, J. Neurosurg. **84**, 203 (1996).
[9]T. Bouwens van der Vlis, O. Schijns, F. Schaper, G. Hoogland, P. Kubben, L. Wagner, R. Rouhl, Y. Temel, and L. Ackermans, Neurosurg. Rev. **42**, 287 (2019).
[10]J.-P. Wang, W. C. Low, and D. Mahendra, U.S. patent US 2016/0303392 A1 (20 October 2016).
[11]M. Jamali, H. Yang, and K.-J. Lee, Appl. Phys. Lett. **96**, 242501 (2010).
[12]T. Koyama *et al.*, Nat. Mater. **10**, 194 (2011).
[13]T. Koyama *et al.*, Appl. Phys. Lett. **98**, 192509 (2011).
[14]D. Moretti *et al.*, Front. Neurosci. **12**, 909 (2018).
[15]M. D. Du, S. L. Guan, L. Gao, S. Y. Lv, S. T. Yang, J. D. Shi, J. F. Wang, H. B. Li, and Y. Fang, Small **15**, 1900582 (2019).
[16]C. Bodart, N. Rossetti, J. Hagler, P. Chevreau, D. Chhin, F. Soavi, S. B. Schougaard, F. Amzica, and F. Cicoira, ACS Appl. Mater. Interfaces **11**, 17226 (2019).
[17]X. Lei *et al.*, J. Neural Eng. **13**, 046016 (2016).
[18]See https://math.nist.gov/oommf/ for "OOMMF code" (2018).
[19]B. J. Gluckman, E. J. Neel, T. I. Netoff, W. L. Ditto, M. L. Spano, and S. J. Schiff, J. Neurophysiol. **76**, 4202 (1996).
[20]J. G. Jefferys, J. Physiol. Lond. **319**, 143 (1981).
[21]B. J. Gluckman, T. I. Netoff, E. J. Neel, W. L. Ditto, M. L. Spano, and S. J. Schiff, Phys. Rev. Lett. **77**, 4098 (1996).
[22]V. Dayal, P. Limousin, and T. Foltynie, J. Parkinsons Dis. **7**, 235 (2017).
[23]T. Trunk, M. Redjdal, A. Kakay, M. F. Ruane, and F. B. Humphrey, J. Appl. Phys. **89**, 7606 (2001).
[24]J. H. Ai, B. F. Miao, L. Sun, B. You, A. Hu, and H. F. Ding, J. Appl. Phys. **110**, 093913 (2011).
[25]N. L. Schryer and L. R. Walker, J. Appl. Phys. **45**, 5406 (1974).
[26]G. S. D. Beach, C. Nistor, C. Knutson, M. Tsoi, and J. L. Erskine, Nat. Mater. **4**, 741 (2005).
[27]G. S. D. Beach, M. Tsoi, and J. L. Erskine, J. Magn. Magn. Mater. **320**, 1272 (2008).
[28]D. C. Ralph and M. D. Stiles, J. Magn. Magn. Mater. **320**, 1190 (2008).
[29]A. Kunz, Appl. Phys. Lett. **94**, 132502 (2009).
[30]M. M. Reich *et al.*, Ann. Clin. Transl. Neur. **2**, 427 (2015).
[31]M. E. Rizou and T. Prodromakis, Biomed. Phys. Eng. Express **4**, Unsp 025016 (2018).
[32]S. W. Lee, F. Fallegger, B. D. F. Casse, and S. I. Fried, Sci. Adv. **2**, e1600889 (2016).